Nuclear Engineering and Technology 54 (2022) 3051–3058

Contents lists available at ScienceDirect

Nuclear Engineering and Technology

journal homepage: www.elsevier.com/locate/net

Original Article

A novel barium oxide-based Iraqi sand glass to attenuate the low gamma-ray energies: Fabrication, mechanical, and radiation protection capacity evaluation

F.H.F. Al-Saeedi [a, **], M.I. Sayyed [b, c], F.L. Kapustin [d], Hanan Al-Ghamdi [e], E.V. Kolobkova [a], O.L. Tashlykov [d], Aljawhara H. Almuqrin [e], K.A. Mahmoud [d, f, *]

[a] Saint-Petersburg State Institute of Technology, Moskovsky pr. 26, St. Petersburg, 190013, Russia
[b] Department of Physics, Faculty of Science, Isra University, Amman, 11622, Jordan
[c] Department of Nuclear Medicine Research, Institute for Research and Medical Consultations, Imam Abdulrahman bin Faisal University, Dammam, 31441, Saudi Arabia
[d] Ural Federal University, 19 Mira St, 620002, Yekaterinburg, Russia
[e] Department of Physics, College of Science, Princess Nourah bint Abdulrahman University, P.O.Box 84428, Riyadh, 11671, Saudi Arabia
[f] Nuclear Materials Authority, P.O Box 530 El-Maadi, Cairo, Egypt

ARTICLE INFO

Article history:
Received 24 January 2022
Received in revised form
2 March 2022
Accepted 12 March 2022
Available online 15 March 2022

Keywords:
Barium oxide
Glass based silica
Monte Carlo simulation
Gamma-ray protection

ABSTRACT

In the present work, untreated Iraqi sand with grain sizes varied between 100 and 200 μm was used to produce a colored glass sample that has shielding features against the low gamma-ray energy. Therefore, a weight of 70–60 wt % sand was mixed with 9–14 wt% B_2O_3, 8–10 wt% Na_2O, 4–6 wt% of CaO, 3–6 wt% Al_2O_3, in addition to 0.3% of Co_2O_3. After melting and annealing the glass sample, the X-ray diffraction spectrometry was applied to affirm the amorphous phase of the fabricated glass samples. Moreover, the X-ray dispersive energy spectrometry was used to measure the chemical composition, and the MH-300A densimeter was applied to measure the fabricated sample's density. The Makishima-Makinzie model was applied to predict the mechanical properties of the fabricated glass. Besides, the Monte Carlo simulation was used to estimate the fabricated glass sample's radiation shielding capacity in the low-energy region between 22.1 and 160.6 keV. Therefore, the simulated linear attenuation coefficient changed between 10.725 and 0.484 cm^{-1}, raising the gamma-ray energy between 22.1 and 160.6 keV. Also, other shielding parameters such as a half-value layer, pure lead equivalent thickness, and buildup factors were calculated.

1. Introduction

Natural sand is a common material used mainly in building applications in countries with hot, dry climates. Usually, sand mainly contains silica-rich quartz. The white sand from the deserts of western Iraq is suitable for glass fabrication due to its high content of silica (approximately 98.5%.) and low content of impurities such as Fe_2O_3. The quartz grain size of the sand in the mentioned region is varied ranged between 100 and 600 μm.

Recently, much effort has been paid to create new talented glass systems with good optical, mechanical, as well as suitable radiation shielding properties. Glass materials were confirmed to have unlimited physical features such as ease of manufacture, high transparency, low cost (especially glasses fabricated from natural silica), and excellent chemical resistance. Furthermore, due to the earlier beneficial features of glass, radiological attention has been directed to the utilization of heavy-weight glass (HWG) in gamma-ray protection applications.

Gamma rays and X-rays are considered the most dangerous type of ionizing radiation due to their high penetration power. Therefore, they can travel miles and ease pass through matter. The transpose of these types of radiation can only be controlled through three main parameters, distance, time of exposure, and the shielding material. The third parameter is the most important.

* Corresponding author. Ural Federal University, 19 Mira St, 620002, Yekaterinburg, Russia.
** Corresponding author.
E-mail addresses: Farhan_fatimah@yahoo.com (F.H.F. Al-Saeedi), karemabdelazeem@yahoo.com (K.A. Mahmoud).

https://doi.org/10.1016/j.net.2022.03.016

Thus, Researchers are focusing on providing adequate protection for workers and patients exposed to radiation daily. A radiation shield is defined as any material that has the ability to attenuate radiation and reduce its intensity to a safe level [1–4]. Recently a lot of articles report the shielding properties of various natural rocks [5–8], various glass types (silicate, borate, phosphate, and tellurite) [9–12], ceramic [13,14], and metallic alloy samples [15–17].

Glass-based SiO_2 is considered one of the common glass-forming agents due to its excellent features. These properties include high thermal stability, high electric field strength, and small cation size [18]. The silicate-based glass properties can be modified using the reinforcing by alkali metals [19]. An early study reported by Warren and Biscoe [20] showed that the alkali silicate glass network included a silicon atom bonded to four oxygen atoms via crosslinked oxygen (BO) and one via non-crosslinked oxygen (NBO). He reported that the remaining silicon atoms bonded to the silicon atoms should be included. When Na_2O is introduced into the Si glass composition, Na cations are present in the random holes throughout the silicon-oxygen network. Nesbitt et al. [21] confirmed that in the case of Na_2O-rich glass, there is an oxygen species called free oxygen O_2, and the amount of O_2 is important mainly in Na_2O-rich Si glass. This free oxygen is urgently needed for the formation of sodium clusters, especially in the case of high concentrations of Na_2O. Further, when intermediate oxides such as zirconium oxide (ZrO_2), CaO, and MgO are added to the silicate glass composition, a glass modifier or glass is added depending on the content in the glass composition. It functions as a forming agent [22]. Introducing ZrO_2 into silicate or borosilicate glass alters chemical and physical features. In brief, it enhances the density, mechanical strength, and chemical resistance and decreases the coefficient of thermal expansion. Changes in glass properties due to the addition of ZrO_2 are often discussed as a result of the support of the glass network by the junction corner connections of [ZrO_6] octahedrons and [SiO_4] tetrahedra in the glass forming network [23]. Several attempts have been made to investigate the effects of zirconium oxide (ZrO_2) on silicate glass's physical properties. For example, Khan et al. [24] reported the role of ZrO_2 on the structural and dielectric features of Y_2O_3 single-bonded CaO borosilicate glass, as well as the radiation shielding capacity for silicate and borosilicate glasses, were modified with heavy metal oxides such as Y_2O_3 and BaO compounds [25,26].

The novelty of this investigation lies in the fabrication of Iraqi silica glass-reinforced barium oxide (BaO) compounds to produce a glass with high mechanical and low energy gamma-ray shielding characteristics. Thus, the mechanical properties of the fabricated glass-based Iraqi sand were estimated using the Makishia-Mackenzie model. Furthermore, the radiation shielding properties for low gamma photon energy were examined using the Monte Carlo simulation.

2. Materials and methods

2.1. Barium based silicate glass fabrications

The natural Iraqi sand from Al-Arma government was collected. It is known that the sands in the studied area contain a concentration of 0.1 wt% of iron oxide (III) for the medium and fine grain sizes' sand. The reason for this is that iron (III) oxide is very brittle compared to quartz sands. Therefore, as a result of transportation, loading, and drilling, it is somewhat exposed to frictional processes, which leads to fracture and fragmentation. In contrast, for the sand with larger grain sizes between 0.1 and 0.2 mm, iron oxide (III) concentration ranged between 0.12 and 0.15 wt%. This ratio is valid only for the production of colored glass. In Iraq, where 70-60% of these sands are used in the production of the glass charge (glass mixture), in addition to 9–14 wt% B_2O_3, 10–8 wt% Na_2O, 4–6 wt% of CaO, 3–6 wt% Al_2O_3, in addition to 0.3% of Co_2O_3. The previously mentioned compounds and sand were mixed, blended, and ground. Then the glass was melted at a temperature of 1580 °C for 30 min. The molten was cast easily poured into a copper mold and annealed at a temperature between 530 and 550 °C to get rid of internal pressures and surface tension of fabricated glass, as described in Fig. 1. The chemical composition of the fabricated glass was determined using the EDX, (see Table 1). Moreover, the densimeter MH-300A with a detection limit of 0.001 g/cm^3 was used to measure the density of the fabricated barium-based silicate glass. The uncertainty in the density measurement was found in the range of ±5%, and the recorded density is 2.645 ± 0.132 g/cm^3**.** After five repetitions, we found that the average density is 2.645 ± 0.132 g/cm^3. The chemical composition of the fabricated glass is an important factor in the present study. Thus, a part of the fabricated glass was crushed, and the highly accurate dispersive energy X-Ray was utilized to determine the chemical composition of the tested samples, as presented in Table 1.

From Fig. 2, the XRD pattern of the fabricated barium-based Iraqi silica glass did not show a crystallinity peak. The lack of widespread humps and sharp peaks indicates the fabricated glass's amorphousness. The X-ray pattern in Fig. 2 shows no continuous/discrete sharp peaks. The XRD pattern of all glasses shows the amorphous hump but at different positions depending on their chemical compositions. The peak of these hump features usually correlates with the intense XRD peak of the major components. Silica exhibits a strong XRD peak at 2theta between 20 and 30°.

2.2. Mechanical properties evaluations

The packing factor (V_i) was estimated with the help of the density (ρ, g/cm^3), chemical composition, and the ionic radiation and coordination number of the elements constating the glass sample. Moreover, the heat of formation (enthalpy) for the compounds constating the fabricated glasses was utilized to calculate the dissociation energy (G_t, kJ/cm^3). Also, the packing density (V_t) was reported with the help of the values of V_i for the fabricated barium oxide-based Iraqi silica glass. Finally, the previously mentioned G_t and V_t were applied in order to calculate the mechanical moduli, Young (Y), Bulk (B), Shear (S), Longitudinal (L) mechanical modulus, using the Makishima-Makenzi method. Moreover, other mechanical properties such as Poisson ratio, Micro-hardness (H, GPa), longitudinal velocity (V_l, cm/s), shear velocity (V_s, cm/s), and softening temperature (T_s, °C) were estimated using the next equations [27–31].

$$V_t = \frac{\rho}{M}\sum_i V_i X_i \quad (1) \tag{1}$$

$$Y = 8.36\, V_t G_t \quad (2) \tag{2}$$

$$B = 10.0\, V_t^2 G_t \quad (3) \tag{3}$$

$$S = \frac{30.0\, V_t^2}{10.2 V_t - 1} G_t \quad (4) \tag{4}$$

$$L = \left[10 + \frac{4}{3}\left(\frac{30}{10.2\, V_t - 1}\right)\right] V_t^2 G_t \quad (5) \tag{5}$$

$$\sigma = \frac{1}{2} - \frac{1}{7.2 V_t} \quad (6) \tag{6}$$

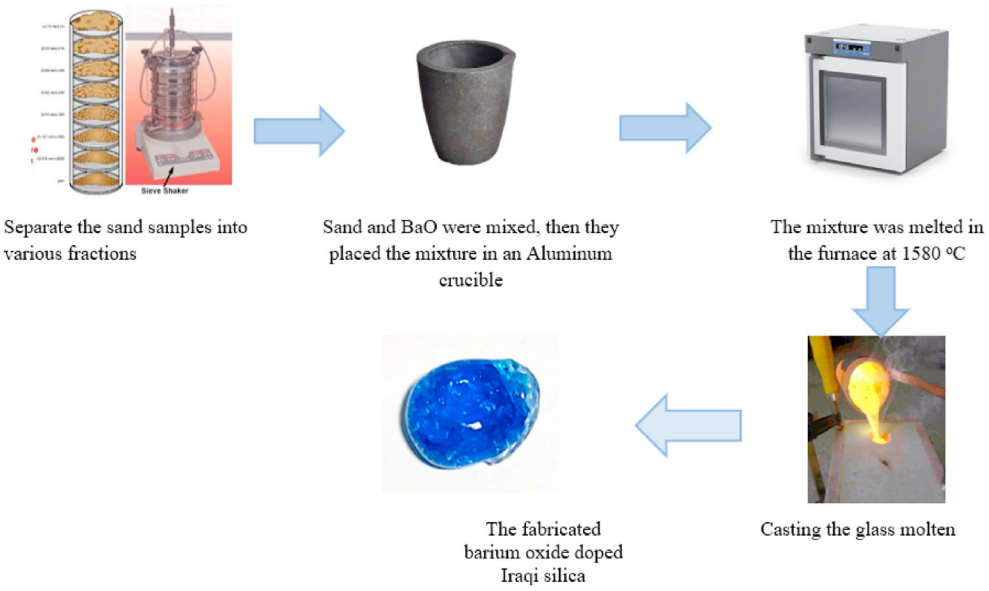

Fig. 1. The barium based Iraqi silica fabrication processes.

Table 1
The chemical composition of the fabricated barium based Iraqi silica.

	Chemical concentration (wt%)
Na_2O	10.902
Al_2O_3	6.193
SiO_2	65.157
K_2O	0.108
CaO	6.358
TiO_2	1.185
Fe_2O_3	0.128
BaO	9.967

$$H = \frac{(1-2\sigma)}{6(1+\sigma)}Y \quad (7) \tag{7}$$

$$T_s(^oC) = \frac{V_s^2 M}{\rho^* C} \quad (8) \tag{8}$$

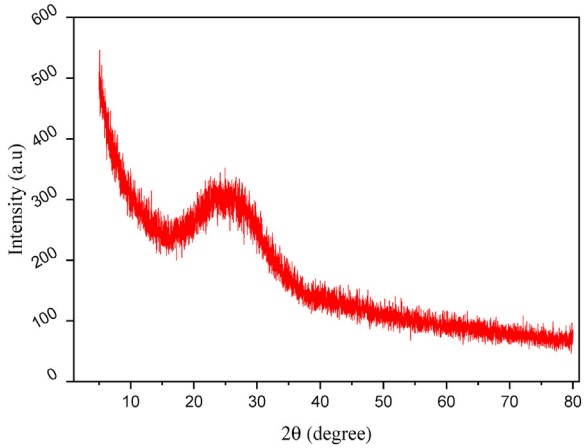

Fig. 2. The X-ray diffraction pattern for the fabricated barium oxide-based Iraqi silica.

2.3. Evaluation of gamma-ray shielding capacity

The Monte Carlo simulation [32] is a common technique for the evaluation of the radiation attenuation parameters for a medium. Hence, we adopted this technique in our current investigation to evaluate the radiation shielding capacity for the prepared glass in the low energy (i.e. between 20.1 and 160.6 keV). The average track length of low-energy gamma photons was estimated based on the Monte Carlo simulation nuclear library ENDF/B-VI.8. The geometry clarifies the simulation cards (cell, source, surface, material, and importance) was described in detail in many previously published papers [33–35] and shown in Fig. 3.

3. Results and discussion

3.1. Mechanical properties

Based on the fabricated glass's chemical composition, density, the heat of enthalpy of the glass consisting compounds, the dissociation energy (G_t) of the fabricated barium-based silica glass was calculated. Moreover, using the ionic radius and the coordination numbers of the elements consisting of the fabricated glasses, the fabricated glass's packing factor (V_i) and packing density were calculated. As illustrated in Table 2, G_t, V_i, and V_t values for the

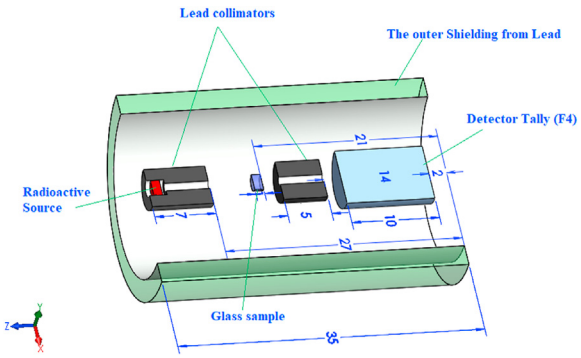

Fig. 3. The Monte Carlo simulation geometry.

Table 2
The physical and mechanical properties of the fabricated barium based Iraqi silica.

Density (g/cm^3)	2.642
Molar mass (g/mol)	65.952
Molar volume (cm^3/mol)	24.963
Packing factor V_i (cm^3/mol)	13.411
Dissociation energy	65.116
Packing density V_t	0.537
Young model (GPa)	69.965
Bulk model (GPa)	45.105
Shear model (GPa)	28.178
Poisson ratio (σ)	0.241
Micro-hardness (GPa)	4.857
Longitudinal model (GPa)	82.675
Longitudinal velocity V_l (m/s)	5593.993
Shear velocity V_s (m/s)	3265.799
Softening temperature Ts (°C)	524.713

fabricated glass are 65.116 kJ/cm^3, 13.411 cm^3/mol, and 0.537, respectively. As a result of the high values of the G_t, the mechanical moduli have values of 69.965 GPa, 45.105 GPa, 28.178 GPa, and 82.675 GPa, for Y, B, S, and L modulus, respectively. In addition, the fabricated glass sample also has a high microhardness (i.e., 4.857 GPa) which is related to the high values of V_t.

3.2. Gamma-ray shielding properties

The fabricated barium-based Iraqi silica linear attenuation coefficient (μ) was estimated via Monte Carlo simulation (MC). Moreover, the MC estimated results were compared to the XCOM results for the same glass composition. Both methods are compatible with differences in the range between ±2%, as shown in Fig. 4. We aimed to study the performance of the barium-based Iraqi silica in shielding the low gamma-ray photons, which are commonly used in medical applications. Thus, the gamma photon energy spectrum was selected to extend between 22.1 and 160.6 keV. As illustrated in Fig. 4, the highest μ recorded for the barium-based Iraqi silica is 10.725 cm^{-1}, achieved at 22.1 keV. Among the examine energy zone, the lowest μ value is 0.484 cm^{-1}, recorded at 160.6 keV. The previous trend in the μ values is related to the photoelectric cross-section, which varied with $Z^{4-5}/E^{3.5}$ [36–38]. Therefore, the average μ values of the fabricated glasses in the studied energy range are around 4.060 cm^{-1} which is suitable for application in the low gamma-ray energy shielding application. Also, around 40 keV, the K-absorption edges that characterized the Ba element appeared [39–41]. This indicates the role of BaO on the shielding performance of the examined sample. Increasing the BaO compound in the fabricated glass-based Iraqi silica causes an increase in the ρ and Z_{eff} of the current glass.

The μ value for the fabricated barium based Iraqi silica glass sample was compared to some of the previously fabricated glasses, at gamma of 59.5 keV, as illustrated in Fig. 5. The μ value for the current sample is 1.025 cm^{-1} which is better than the μ values for NBSM0 (0.708 cm^{-1}) and NBSM2 (0.621 cm^{-1}) [42]. On contrast, the current sample has μ value lower than that recorded for samples BTPZE, TPBE, BTPLE, BTPSE, BTPCE, BTNKD-X (where X = Li, Ca, Zn, Sr and Ba), 0NBDB, and 20NBDB with μ values of 9.556, 17.874, 7.713, 10.327, 8.316, 5.050, 5.635, 7.424, 6.958, 10.020, 14.198, and 12.080 cm^{-1} [43–45]. The high μ values reported for the previously fabricated glasses is due to the high percentage of dense compounds such as PbO, $BaCO_3$, TeO_2, and Nb_2O_5.

Based on the simulated μ values as well as the measured density for the fabricated barium oxide-based Iraqi silica glass, the mass attenuation coefficient (μ_m, cm^2/g) was calculated, as presented in Fig. 6. The μ_m highest value is 4.060 cm^2/g and decreased rapidly to 0.183 cm^2/g between 22.1 and 160.6 keV, respectively. The variation of the μ_m against the energy is the same as early presented in the linear attenuation paragraph.

Moreover, the half-value thickness ($\Delta_{0.5}$) for the silica-based glass was calculated, as presented in Fig. 6. The $\Delta_{0.5}$ is the thickness that has the ability to diminish the photon flux emitted from the radioactive source to half of its initial value. Between 22.1 and 160.6 keV, the $\Delta_{0.5}$ thickness increases from 0.065 to 1.431 cm with an average value of 0.359 cm. This small $\Delta_{0.5}$ value makes the fabricated glasses one of the more suitable candidates for protection purposes uses in medical applications.

The thickness equivalent to 0.5 cm of lead (D_{eq}) at this energy region between 22.1 and 160.6 keV was calculated, as illustrated in Fig. 6. The D_{eq} varied between 35.253 and 19.928 cm in the studied energy interval with an average of 28.473 cm. The high D_{eq} values are related to the fabricated glass's lower density and μ values compared to lead density and μ values at the same gamma photon energies. Around gamma-ray energy of 40 keV, the D_{eq} for the fabricated glass dropped to 10.5 cm due to the increase of μ values for the current glass and this is related to the absorption K-edges of Ba.

The transmission factor (TF) and radiation shielding capacity (RSC) are two important factors related to the photon's penetration. Both factors were calculated based on the glass thickness and the μ

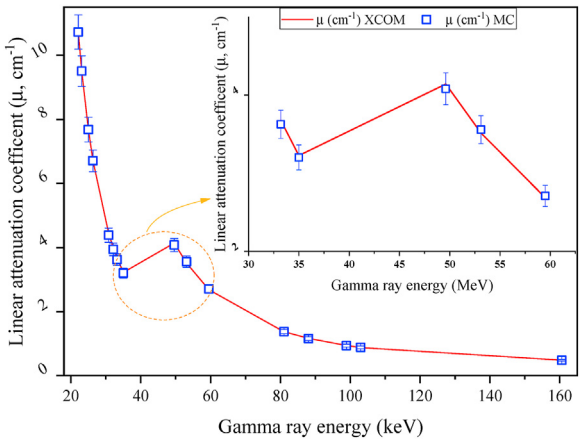

Fig. 4. The linear attenuation coefficient of the fabricated barium based Iraqi silica in the gamma-ray energy range.

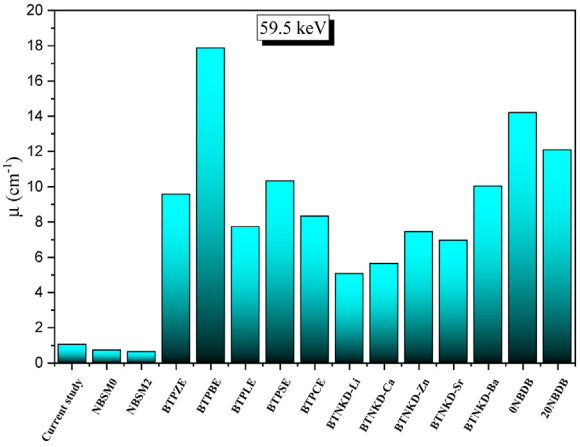

Fig. 5. Comparison between the linear attenuation coefficient of the fabricated glasses and some of the previously prepared glasses.

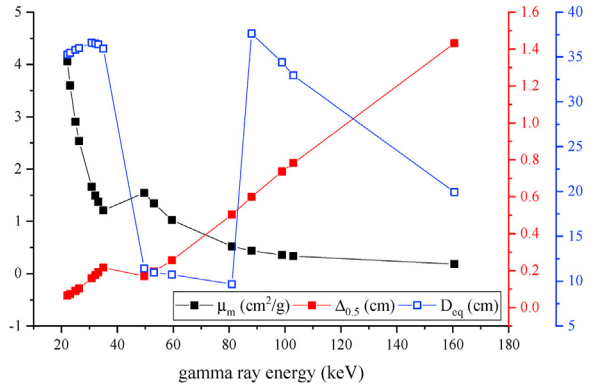

Fig. 6. Variation of the mass attenuation coefficient, half-value thickness ($\Delta_{0.5}$, cm) and lead equivalent thickness (D_{eq}) with the energy in the energy interval between 20 and 180 keV.

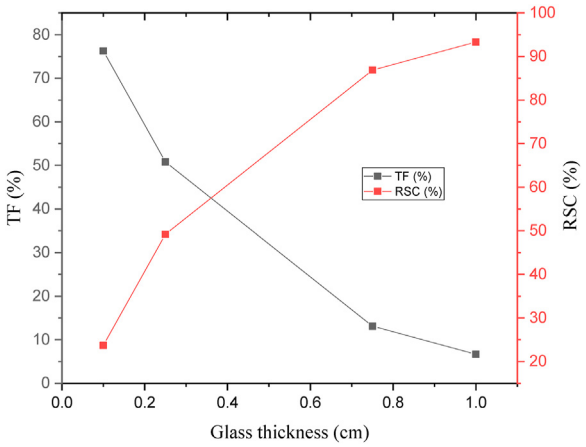

Fig. 8. The transmission factor (TF) and radiation shielding capacity (RSC) versus the glass thickness.

of the present barium-based Iraqi silica glass. Fig. 7 clarifies the change in TF and RSC versus the energy for a sample with a thickness of 0.5 cm. Clearly, the TF values increase, raising the energy between 22.1 and 160.6 keV. The TF values increase from 0.469% to 78.496%, with an average of 27.232%. This increase in the TF value is related to diminishing the photoelectric interaction and beginning the CS interaction with increasing the energy. Thus, the interaction was associated with the loss of a small part of photon energy, and the photons have enough energy to escape from the glass thickness. On the other hand, the RSC decreases gradually, raising the photon energy. This trend is also attributed to the CS increase inside the glass. In this regard, the RSC for the fabricated barium-based Iraqi silica decreased from 99.530% to 21.503%, between 22.1 and 160.6 keV, respectively.

Both TF and RSC depended on the glass thickness, as clarified in Fig. 8. At 59.5 keV, the TF values decrease with a following order 76.269%, 50.801%, 13.111%, and 60.660%, while the RSC increases in the order of 23.731%, 49.199%, 86.889%, and 93.340%, growing the glass thickness between 0.1, 0.25, 0.75, and 1 cm, respectively. Increasing the thickness of the sample means more impacts and collisions were carried out between the photons and the glass atoms, which causes a high loss in the energy of the incident photos.

The effective and equivalent atomic numbers and the electron density (A_{eff}) were calculated theoretically based on the Phy-X/PSD [46] program between 15 and 200 keV, as clarified in Fig. 9. Both Z_{eff} and A_{eff} attach high values at low gamma photon energies followed by a huge increase around 40 keV. After that, they are reduced highly by raising the gamma photon energy. This reduction in Z_{eff} and A_{eff} is related to the interaction mode, where the photoelectric interaction is changed with $Z^{4-5}/E^{3.5}$ in the studied energy range. For example, Z_{eff} decreases from 21.11 to 21.76. Simultaneously, the A_{eff} decreases from 5.782 E+23 to 3.495 E+23 electons/g.

In a separate context, the Z_{eq} depends mainly on the ratio between partial Compton scattering μm to the total μm for the fabricated glass. Hence, Fig. 9 shows a low Z_{eff} value in the low energy region extending to 30 keV, where the photoelectric interaction is the main. After that (above 40 keV), the Compton scattering starts to appear inside the glass. Thus, the Z_{eq} values increase regard with raising the Compton scattering interaction. For example, the Z_{eq} values were varied between 14.54 and 15.09, raising the gamma photon energy between 15 and 30 keV. After that, a high increase was observed, where the Z_{eq} values varied between 22.63 and 26.9 between 40 and 200 keV, respectively.

The buildup factor (BUF) for the incident photons was divided into exposure and energy absorption buildup factors (EBF and EABF). The EBF is related to the accumulated photons in the air between the detector and the radioactive source, while the EABF calculates the predicted accumulated photons inside the shield. Both BUFs were estimated for the energy ranging from 15 to 200 keV, as clarified in Fig. 10 a and b. The photoelectric effect

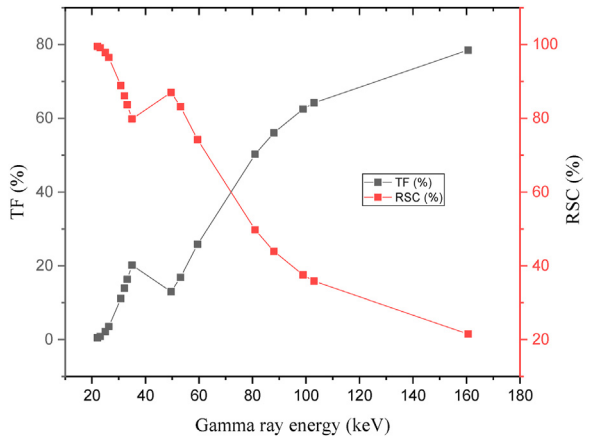

Fig. 7. The TF and RSC as a function of the gamma photon energy in the energy interval between 20 and 180 keV.

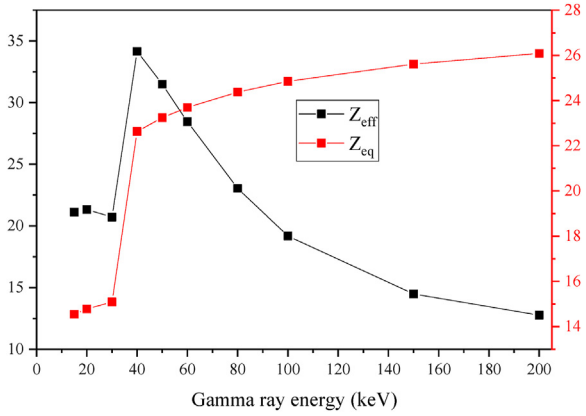

Fig. 9. The effective and equivalent atomic numbers versus the gamma-ray photon energy in the interval between 15 and 200 keV.

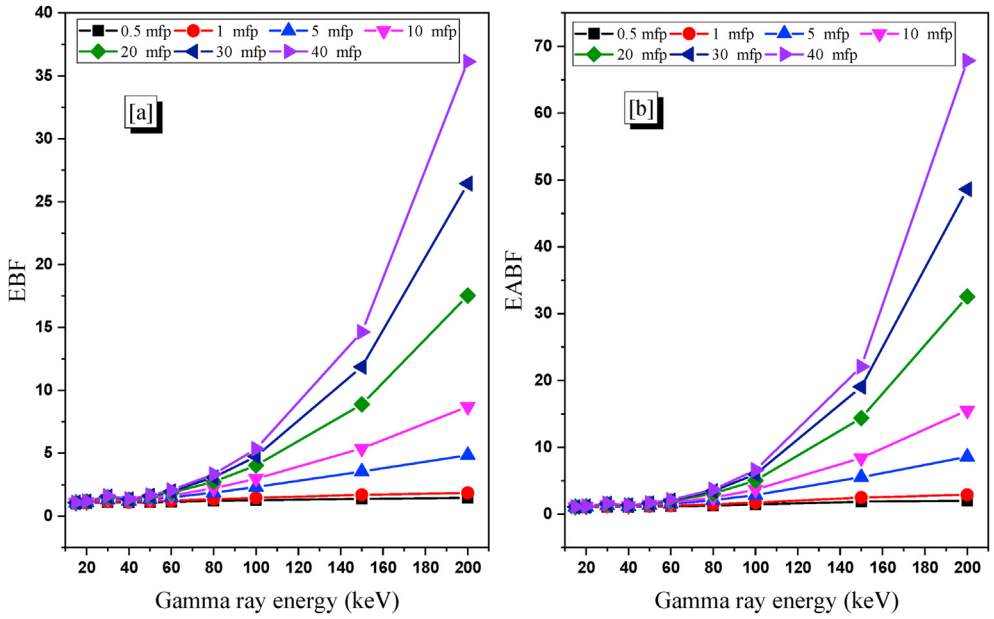

Fig. 10. Variation of the buildup factors versus the gamma-ray photon energy in the interval between 15 and 200 keV.

influenced the values of both parameters in the studied energy interval. The photoelectric interaction absorbs the total energy of photons to liberate an electron from the outer shell of atoms. Hence, the number of photons accumulated inside the glass and air was dropped to its lower values until the Compton scattering appeared. Above 100 keV, the air and glass sample accumulation start to rise progressively with raising the energy under the effect of Compton scattering, which absorbs only a small part of the gamma photon energy. The accumulation of photons was also affected by the penetration depth in the unit of mfp. Where increasing the penetration depth causes an increase in the accumulation of photons (i.e., EBF and EABF), as presented in Fig. 11. The increase of EBF and EABF is relatively small for small penetration depths. After that, increasing the penetration depth causes an increased path length of the incident gamma photons, increasing the probability of photons' accumulation. At 60 keV, the EBF values increase between 1.133 and 2.061. Simultaneously, the EABF increases between 1.153 and 2.119, raising the penetration depth between 0.5 and 40 mfp, respectively. The last observation is that the accumulation of photons in glass

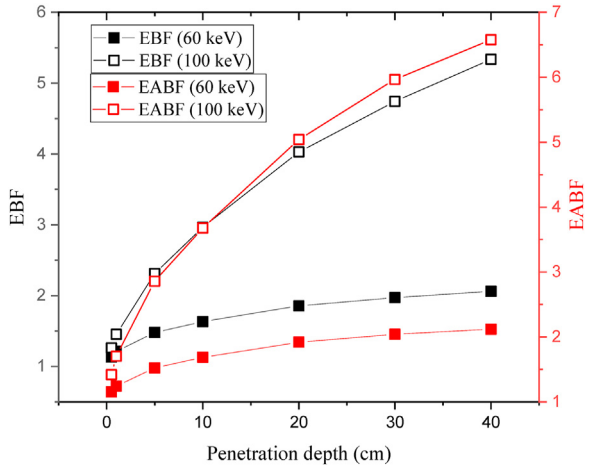

Fig. 11. Variation of buildup factors versus the penetration depth.

EBF is slightly higher than that achieved in air. This is related to the Z_{eff} of the fabricated glass, which is higher than the Z_{eff} of air.

4. Conclusions

The present work presented the method for fabrication of a barium oxide-based Iraqi sand to be applied in the radiation protection applications for the low energy gamma photons. The melting process was performed at a melting temperature of 1580 °C, while the annulling was performed in the energy range between 530 and 550 °C. In addition, the amorphous phase for the fabricated glass was confirmed using X-ray diffraction. The mechanical properties of the fabricated glass were checked using the Makishima-Makinzie method, where the mechanical moduli values are 6.965 GPa, 45.105 GPa, 28.178 GPa, and 82.675 GPa, for Y, B, S, and L, respectively. Besides, the microhardness of the fabricated barium oxide-based Iraqi silica glass reaches 4.857 GPa. The gamma-ray shielding capacity was examined using the MC simulation between 22.1 and 160.6 keV. The μ values decreased between 10.725 and 0.484 cm^{-1} while the $\Delta_{0.5}$ increases from 0.065 to 1.431 cm when the gamma photo energy increased between 22.1 and 160.6 keV, respectively. Besides the suitable shielding capacity, the high microhardness value makes the present barium oxide-based Iraqi sand a good candidate for radiation shielding applications in medical and low gamma-ray energy applications.

Declaration of competing interest

The authors declare that they have no known competing financial interests or personal relationships that could have appeared to influence the work reported in this paper.

Acknowledgement

The authors express their gratitude to Princess Nourah bint Abdulrahman University Researchers Supporting Project number (PNURSP2022R28), Princess Nourah bint Abdulrahman University, Riyadh, Saudi Arabia.

References

[1] K.A. Naseer, K. Marimuthu, K.A. Mahmoud, M.I. Sayyed, Impact of Bi2O3 modifier concentration on barium–zincborate glasses: physical, structural, elastic, and radiation-shielding properties, The European Physical Journal Plus 136 (2021) 116, https://doi.org/10.1140/epjp/s13360-020-01056-6.

[2] A.S. Abouhaswa, M.I. Sayyed, K.A. Mahmoud, Y. Al-Hadeethi, Direct influence of mercury oxide on structural, optical and radiation shielding properties of a new borate glass system, Ceram. Int. 46 (2020) 17978–17986, https://doi.org/10.1016/j.ceramint.2020.04.112.

[3] R. Divina, K. Marimuthu, K.A. Mahmoud, M.I. Sayyed, Physical and structural effect of modifiers on dysprosium ions incorporated boro-tellurite glasses for radiation shielding purposes, Ceram. Int. 46 (2020) 17929–17937, https://doi.org/10.1016/j.ceramint.2020.04.102.

[4] S. Islam, K.A. Mahmoud, M.I. Sayyed, B. Alim, M. Rahman, A.S. Mollah, Study on the radiation attenuation properties of locally available bees-wax as a tissue equivalent bolus material in radiotherapy, Radiat. Phys. Chem. (2019), 108559, https://doi.org/10.1016/j.radphyschem.2019.108559.

[5] N.K. Libeesh, K.A. Naseer, S. Arivazhagan, K.A. Mahmoud, M.I. Sayyed, M.S. Alqahtani, E.S. Yousef, Multispectral remote sensing for determination the Ultra-mafic complexes distribution and their applications in reducing the equivalent dose from the radioactive wastes, The European Physical Journal Plus 137 (2022) 267, https://doi.org/10.1140/epjp/s13360-022-02473-5.

[6] N.K. Libeesh, K.A. Naseer, S. Arivazhagan, A.F. Abd El-Rehim, K.A. Mahmoud, M.I. Sayyed, M.U. Khandaker, Advanced nuclear radiation shielding studies of some mafic and ultramafic complexes with lithological mapping, Radiat. Phys. Chem. 189 (2021), 109777, https://doi.org/10.1016/j.radphyschem.2021.109777.

[7] N.K. Libeesh, K.A. Naseer, S. Arivazhagan, A.F.A. El-Rehim, G. ALMisned, H.O. Tekin, Characterization of Ultramafic–Alkaline–Carbonatite complex for radiation shielding competencies: an experimental and Monte Carlo study with lithological mapping, Ore Geol. Rev. 142 (2022), 104735, https://doi.org/10.1016/j.oregeorev.2022.104735.

[8] N.K. Libeesh, K.A. Naseer, K.A. Mahmoud, M.I. Sayyed, S. Arivazhagan, M.S. Alqahtani, E.S. Yousef, M.U. Khandaker, Applicability of the multispectral remote sensing on determining the natural rock complexes distribution and their evaluability on the radiation protection applications, Radiat. Phys. Chem. 193 (2022), 110004, https://doi.org/10.1016/j.radphyschem.2022.110004.

[9] S. Singh, A. Kumar, D. Singh, K.S. Thind, G.S. Mudahar, Barium-borate-flyash glasses: as radiation shielding materials, Nucl. Instrum. Methods Phys. Res. Sect. B Beam Interact. Mater. Atoms 266 (2008) 140–146, https://doi.org/10.1016/j.nimb.2007.10.018.

[10] M.Y. Hanfi, M.I. Sayyed, E. Lacomme, I. Akkurt, K.A. Mahmoud, The influence of MgO on the radiation protection and mechanical properties of tellurite glasses, Nucl. Eng. Technol. (2020), https://doi.org/10.1016/j.net.2020.12.012.

[11] A. Kumar, A. Jain, M.I. Sayyed, F. Laariedh, K.A. Mahmoud, J. Nebhen, M.U. Khandaker, M.R.I. Faruque, Tailoring bismuth borate glasses by incorporating PbO/GeO2 for protection against nuclear radiation, Sci. Rep. 11 (2021) 1–14, https://doi.org/10.1038/s41598-021-87256-1.

[12] M.H. Kharita, R. Jabra, S. Yousef, T. Samaan, Shielding properties of lead and barium phosphate glasses, Radiat. Phys. Chem. 81 (2012) 1568–1571, https://doi.org/10.1016/j.radphyschem.2012.05.002.

[13] E. Hannachi, K.A. Mahmoud, A.H. Almuqrin, M.I. Sayyed, Y. Slimani, Evaluation of the radiation-protective properties of Bi (Pb)–Sr–Ca–Cu–O ceramic prepared at different temperatures with silver inclusion, Materials 15 (2022) 1034, https://doi.org/10.3390/ma15031034.

[14] E. Hannachi, K.A. Mahmoud, M.I. Sayyed, Y. Slimani, Effect of sintering conditions on the radiation shielding characteristics of YBCO superconducting ceramics, J. Phys. Chem. Solid. 164 (2022), 110627, https://doi.org/10.1016/j.jpcs.2022.110627.

[15] J. Singh, H. Singh, J. Sharma, T. Singh, P.S. Singh, Fusible alloys: a potential candidate for gamma rays shield design, Prog. Nucl. Energy 106 (2018) 387–395, https://doi.org/10.1016/j.pnucene.2018.04.002.

[16] F. Akman, M.R. Kaçal, M.I. Sayyed, H.A. Karataş, Study of gamma radiation attenuation properties of some selected ternary alloys, J. Alloys Compd. 782 (2019) 315–322, https://doi.org/10.1016/j.jallcom.2018.12.221.

[17] E. Şakar, M. Büyükyıldız, B. Alım, B.C. Şakar, M. Kurudirek, Leaded brass alloys for gamma-ray shielding applications, Radiat. Phys. Chem. 159 (2019) 64–69, https://doi.org/10.1016/j.radphyschem.2019.02.042.

[18] G. El-Damrawi, K. Abd-El-Nour, R.M. Ramadan, Structural and dielectric studies on Na2O-PbO-SiO2 glasses, Silicon 11 (2019) 495–500, https://doi.org/10.1007/s12633-018-9863-7.

[19] Y. Al-Hadeethi, M.S. Al-Buriahi, M.I. Sayyed, Bioactive glasses and the impact of Si3N4 doping on the photon attenuation up to radiotherapy energies, Ceram. Int. 46 (2020) 5306–5314, https://doi.org/10.1016/j.ceramint.2019.10.281.

[20] B.E. Warren, J. Biscce, The structure OF silica glass BY X-ray diffraction studies, J. Am. Ceram. Soc. 21 (1938) 49–54, https://doi.org/10.1111/j.1151-2916.1938.tb15742.x.

[21] H.W. Nesbitt, G.M. Bancroft, G.S. Henderson, R. Ho, K.N. Dalby, Y. Huang, Z. Yan, Bridging, non-bridging and free (O2−) oxygen in Na2O-SiO2 glasses: an X-ray photoelectron spectroscopic (XPS) and nuclear magnetic resonance (NMR) study, J. Non-Cryst. Solids 357 (2011) 170–180, https://doi.org/10.1016/j.jnoncrysol.2010.09.031.

[22] A. Novatski, A. Steimacher, A.N. Medina, A.C. Bento, M.L. Baesso, L.H.C. Andrade, S.M. Lima, Y. Guyot, G. Boulon, Relations among nonbridging oxygen, optical properties, optical basicity, and color center formation in CaO–MgO aluminosilicate glasses, J. Appl. Phys. 104 (2008), 094910, https://doi.org/10.1063/1.3010306.

[23] G. Calas, L. Galoisy, L. Cormier, G. Ferlat, G. Lelong, The structural properties of cations in nuclear glasses, Procedia Mater. Sci. 7 (2014) 23–31, https://doi.org/10.1016/j.mspro.2014.10.005.

[24] S. Khan, G. Kaur, K. Singh, Effect of ZrO2 on dielectric, optical and structural properties of yttrium calcium borosilicate glasses, Ceram. Int. 43 (2017) 722–727, https://doi.org/10.1016/j.ceramint.2016.09.219.

[25] O.L. Tashlykov, S.G. Vlasova, I.S. Kovyazina, K.A. Mahmoud, Repercussions of yttrium oxides on radiation shielding capacity of sodium-silicate glass system: experimental and Monte Carlo simulation study, The European Physical Journal Plus 136 (2021) 428, https://doi.org/10.1140/epjp/s13360-021-01420-0.

[26] M.H.A. Mhareb, M. Alqahtani, Y.S.M. Alajerami, F. Alshahri, M.I. Sayyed, K.A. Mahmoud, N. Saleh, N. Alonizan, M.S. Al-Buriahi, K.M. Kaky, Ionizing radiation shielding features for titanium borosilicate glass modified with different concentrations of barium oxide, Mater. Chem. Phys. 272 (2021), 125047, https://doi.org/10.1016/j.matchemphys.2021.125047.

[27] A. Makishima, J.D. Mackenzie, Direct calculation of Young's moidulus of glass, J. Non-Cryst. Solids 12 (1973) 35–45, https://doi.org/10.1016/0022-3093(73)90053-7.

[28] A. Makishima, J.D. Mackenzie, Calculation of bulk modulus, shear modulus and Poisson's ratio of glass, J. Non-Cryst. Solids 17 (1975) 147–157, https://doi.org/10.1016/0022-3093(75)90047-2.

[29] A. Mohajerani, V. Martin, D. Boyd, J.W. Zwanziger, On the mechanical properties of lead borate glass, J. Non-Cryst. Solids 381 (2013) 29–34, https://doi.org/10.1016/j.jnoncrysol.2013.09.015.

[30] A. Acikgoz, G. Demircan, D. Yılmaz, B. Aktas, S. Yalcin, N. Yorulmaz, Structural, mechanical, radiation shielding properties and albedo parameters of alumina borate glasses: role of CeO2 and Er2O3, Mater. Sci. Eng. B 276 (2022), 115519, https://doi.org/10.1016/j.mseb.2021.115519.

[31] E. Nabhan, Mechanical and structural properties of zinc − sodium - phosphate glasses doped with Cu_2O, Am. J. Phys. Appl. 4 (2016) 145, https://doi.org/10.11648/j.ajpa.20160406.12.

[32] X-5 Monte Carlo Team, MCNP — A General Monte Carlo N-Particle Transport Code, Version 5, La-Ur-03-1987. II, 2003.

[33] K.A. Mahmoud, Y.S. Rammah, Investigation of gamma-ray shielding capability of glasses doped with Y, Gd, Nd, Pr and Dy rare earth using MCNP-5 code, Physica B: Phys. Condens. Matter (2019), 411756, https://doi.org/10.1016/j.physb.2019.411756.

[34] F.I. El-Agawany, O.L. Tashlykov, K.A. Mahmoud, Y.S. Rammah, The radiation-shielding properties of ternary SiO2–SnO–SnF2 glasses: simulation and theoretical study, Ceram. Int. 46 (2020) 23369–23378, https://doi.org/10.1016/j.ceramint.2020.04.042.

[35] Y.S. Rammah, K.A. Mahmoud, E. Kavaz, A. Kumar, F.I. El-Agawany, The role of PbO/Bi2O3 insertion on the shielding characteristics of novel borate glasses, Ceram. Int. 46 (2020) 23357–23368, https://doi.org/10.1016/j.ceramint.2020.04.018.

[36] R. Kurtulus, T. Kavas, K.A. Mahmoud, M.I. Sayyed, A comprehensive examination of zinc-boro-vanadate glass reinforced with Ag2O in physical, optical, mechanical, and radiation shielding aspects, Appl. Phys. Mater. Sci. Process 127 (2021) 1–13, https://doi.org/10.1007/s00339-021-04282-6.

[37] R. Divina, K. Marimuthu, K.A. Mahmoud, M.I. Sayyed, Physical and structural effect of modifiers on dysprosium ions incorporated boro-tellurite glasses for radiation shielding purposes, Ceram. Int. 46 (2020) 17929–17937, https://doi.org/10.1016/j.ceramint.2020.04.102.

[38] A.M Abu El-Soad, M.I Sayyed, K.A. Mahmoud, E Şakar, E.G Kovaleva, Simulation studies for gamma ray shielding properties of Halloysite nanotubes using MCNP-5 code, Appl. Radiat. Isot . 154 (2019), 108882, https://doi.org/10.1016/j.apradiso.2019.108882.

[39] Y. Al-Hadeethi, M.I. Sayyed, BaO–Li2O–B2O3 glass systems: potential utilization in gamma radiation protection, Prog. Nucl. Energy 129 (2020), 103511, https://doi.org/10.1016/j.pnucene.2020.103511.

[40] H.A. Saudi, S.U. El-Kameesy, Investigation of modified zinc borate glasses doped with BaO as a nuclear radiation-shielding material, Radiat. Detect. Technol. Methods 2 (2018) 1–7, https://doi.org/10.1007/s41605-018-0075-x.

[41] S. Kaewjaeng, J. Kaewkhao, P. Limsuwan, U. Maghanemi, Effect of BaO on optical, physical and radiation shielding properties of SiO2-B2O3-Al2O3-CaO-Na2O glasses system, Procedia Eng. 32 (2012) 1080–1086, https://doi.org/10.1016/j.proeng.2012.02.058.

[42] M.S.I. Koubisy, KhS. Shaaban, E.A.A. Wahab, M.I. Sayyed, K.A. Mahmoud, Synthesis, structure, mechanical and radiation shielding features of 50SiO2–(48 + X) Na2B4O7–(2 − X) MnO2 glasses, The European Physical Journal Plus 136 (2021) 156, https://doi.org/10.1140/epjp/s13360-021-01125-4.

[43] P.E. Teresa, K.A. Naseer, T. Piotrowski, K. Marimuthu, D.A. Aloraini, A.H. Almuqrin, M.I. Sayyed, Optical properties and radiation shielding studies of europium doped modifier reliant multi former glasses, Optik 247 (2021), 168005, https://doi.org/10.1016/j.ijleo.2021.168005.

[44] K.A. Naseer, G. Sathiyapriya, K. Marimuthu, T. Piotrowski, M.S. Alqahtani, E.S. Yousef, Optical, elastic, and neutron shielding studies of Nb2O5 varied Dy3+ doped barium-borate glasses, Optik 251 (2022), 168436, https://

doi.org/10.1016/j.ijleo.2021.168436.
[45] P. Evangelin Teresa, K.A. Naseer, K. Marimuthu, H. Alavian, M.I. Sayyed, Influence of modifiers on the physical, structural, elastic and radiation shielding competence of Dy3+ ions doped Alkali boro-tellurite glasses, Radiat. Phys. Chem. 189 (2021) 109741, https://doi.org/10.1016/j.radphyschem.2021.109741.
[46] E. Şakar, Ö.F. Özpolat, B. Alım, M.I. Sayyed, M. Kurudirek, Phy-X/PSD: development of a user friendly online software for calculation of parameters relevant to radiation shielding and dosimetry, Radiat. Phys. Chem. 166 (2020), https://doi.org/10.1016/j.radphyschem.2019.108496.